THE JOURNAL OF PHYSICAL CHEMISTRY C

pubs.acs.org/JPCC Article

Efficient Photoinduced Energy Transfer in Porphyrin-Based Nanomaterials

Tony E. Karam, Noureen Siraj, Jeewan C. Ranasinghe, Paulina E. Kolic, Bishnu P. Regmi, Isiah M. Warner, and Louis H. Haber*

Cite This: J. Phys. Chem. C 2020, 124, 24533−24541

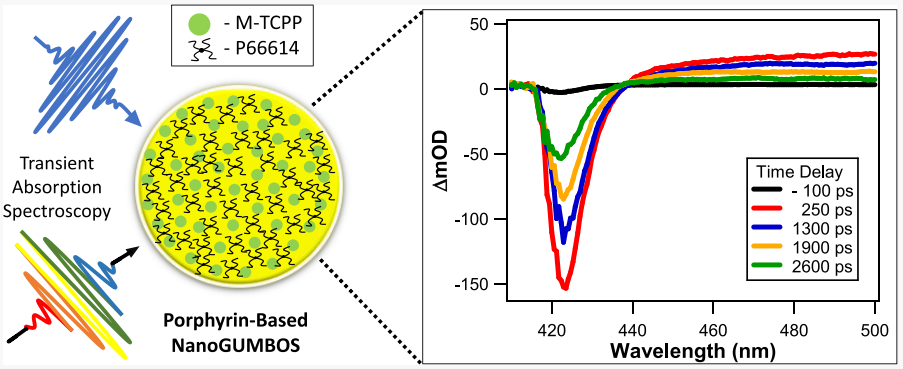

ABSTRACT: Synthesis, characterization, and ultrafast dynamics of porphyrin- and zinc porphyrin-based nanomaterials are reported. Spherical nanoparticles composed of a group of uniform materials based on organic salts (nanoGUMBOS) are prepared from either porphyrin or zinc porphyrin with trihexyl(tetradecyl)phosphonium in aqueous colloidal suspension with sizes of approximately 50 nm in diameter. Ultrafast excited-state dynamics of porphyrin and zinc porphyrin nanoGUMBOS in water are measured using transient absorption spectroscopy with 400 nm excitation. Results are compared to corresponding measurements of the porphyrin molecular dye parent compounds in water. Porphyrin and zinc porphyrin have long-lived excited states arising from intersystem crossing of the first-excited singlet S_1 state to the triplet T_1 state. These excited-state lifetimes are significantly faster in porphyrin-based nanoGUMBOS as compared to the corresponding porphyrin molecules due to intermolecular energy transfer, electronic delocalization, and altered chemical environments of the nanomaterials. Additionally, these results demonstrate that porphyrin-based nanoGUMBOS are promising nanomaterials for light harvesting in solar cells and optoelectronics.

1. INTRODUCTION

Organic and organometallic nanomaterials have drawn great interest due to their many potential applications including photothermal cancer therapy,[1,2] biosensing,[3] and optoelectronics.[4] A group of uniform materials based on organic salts or GUMBOS represents an emerging class of organic and organometallic materials that provides a wide range of controllable chemical, physical, and optoelectronic characteristics.[5] Colloidal nanoparticles prepared from GUMBOS are termed nanoGUMBOS and are scientifically interesting due to their facile synthesis, highly tunable photophysical properties, and extended list of applications in biomedical imaging,[6] antibiotics,[7,8] cancer therapy,[9] molecular sensing,[10−12] organic light-emitting diodes,[13,14] and photovoltaics.[15] Porphyrin-based nanoGUMBOS have been recently investigated and demonstrated to be promising candidates as photosensitizers for dye-sensitized solar cells and optoelectronics.[16] However, a better understanding of the fundamental photophysical properties of these nanomaterials is needed for the design and optimization of new light-harvesting and optoelectronic devices.

We have previously investigated the ultrafast excited-state dynamics of different types of nanoGUMBOS using transient absorption spectroscopy.[17,18] In one study, we reported observation of tunable intermolecular energy transfer in crystalline ruthenium bipyridine-−bis-(pentafluoroethylsulfonyl)imide ($[Ru(bipy)_3][BETI]_2$) nanoGUMBOS in colloidal suspension in water.[17] Size-dependent relaxation dynamics were observed in these nanoGUMBOS,

Received: October 2, 2020
Published: October 21, 2020

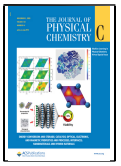

https://dx.doi.org/10.1021/acs.jpcc.0c08985
J. Phys. Chem. C 2020, 124, 24533−24541

characterized by decay dynamics similar to the $Ru(bipy)_3Cl_2$ dye with an added relaxation pathway from intermolecular energy transfer.[17] Additionally, size-dependent phonon oscillations were observed, where the phonon frequency increases as the nanoparticle size increases. This anomalous phonon trend suggests a very low coupling between electronic and phonon degrees of freedom and strong hydrophobic interactions with the aqueous solvent.[17] In a second study, brilliant green−bis(pentafluoroethylsulfonyl)imide ([BG][BETI]) nanoGUMBOS demonstrated slower relaxation dynamics than the BG molecular dye due to the steric hindrance of the torsional degrees of freedom of the phenyl rings around the central carbon in the nanoGUMBOS environment while also displaying enhanced nonlinear optical signals.[18] Understanding the excited-state dynamics of different porphyrin-based nanoGUMBOS is essential for the development and optimization of various optoelectronic applications. In this respect, porphyrin nanoGUMBOS provide a new route for the synthesis of highly tunable functional organic nanomaterials with enhanced photonic properties.

Porphyrin molecular dyes are particularly attractive due to their optical and chemical tunability as well as their highly efficient electron transfer in donor−acceptor configurations, making them promising candidates for advanced dye-sensitized solar cells and optoelectronic devices.[19−22] Additionally, porphyrin dyes can be easily altered by changing the central hydrogen atoms in the heterocyclic structure with different metal ions such as Zn^{2+}, Co^{2+}, and Cu^{2+}. These M-porphyrin-based dyes can be used for the development of artificial light-harvesting antennae that mimic photosynthesis by transferring the absorbed photon energy to a reaction center.[23] For example, zinc porphyrin-sensitized solar cells with a cobalt(II/III)-based redox electrolyte previously recorded an excellent conversion efficiency of 12.3%.[19] Several porphyrin-based synthetic strategies have been utilized for photovoltaics including configurations based on arrays,[24,25] dimers,[26] dendrimers,[27] controlled aggregation,[28] and supramolecular assemblies.[29,30] These synthetic strategies require strong absorbance in the visible region and enhanced electron transfer for efficient photovoltaic designs.[31,32] Porphyrin hexamers have also been studied due to their near-infrared luminescence for organic light-emitting diodes.[33] The unique chemical and optical properties of porphyrins lead to an extensive list of potential applications including photodynamic therapy,[34−37] catalysis,[38−41] and optoelectronics.[19,42] Excited-state dynamics of porphyrin molecular dyes have been studied using various ultrafast pump-probe spectroscopic techniques.[43−47] Additionally, excited-state relaxation processes and interfacial energy transfer mechanisms of porphyrin dyes in solution and attached to substrates have been investigated using ultrafast spectroscopy.[21,26,28] The emerging field of molecular-based nanomaterials, such as nanoGUMBOS, provides the ability to study how molecular photophysical properties are altered as individual molecules are restructured into size-controlled nanomaterials for potentially enhanced optoelectronic applications.[16−18]

In this article, we report investigations of excited-state relaxation dynamics of colloidal trihexyl(tetradecyl)-phosphonium porphyrin ($[P66614]_4$[M-TCPP]) nanoGUMBOS, with M = H_2 and Zn, using ultrafast pump-probe time-resolved transient absorption spectroscopy with pump pulse excitation at 400 nm and white light continuum femtosecond probe pulses. Transient absorption results obtained for these nanoGUMBOS are compared to corresponding results acquired from aqueous solutions of the M-porphyrin parent compound molecular dyes. In the nanoGUMBOS samples, additional efficient energy transfer relaxation pathways are observed, leading to significantly shorter excited-state lifetimes. In addition, the excited-state dynamics of $[P66614]_4$[Zn-TCPP] nanoGUMBOS are considerably faster than those of the molecular dye due to an increase in spin−orbit coupling and electronic delocalization caused by the metal center, leading to enhanced energy transfer in excited-state relaxation dynamics. By incorporating our previous work,[17,18] these studies provide important new details on the photodynamics of different types of nanoGUMBOS for comparisons between amorphous and crystalline structures, between long-lived and short-lived excited states, and between porphyrins with and without a metal center. In general, our results show that nanoGUMBOS are highly attractive for designing new, efficient light-harvesting nanomaterials. The use of organic or organometallic nanoparticles of this type in solar cell devices is advantageous due to their large surface-to-volume ratios, leading to expected increased energy conversion efficiencies. These transient absorption spectroscopy studies provide a fundamental understanding of ultrafast processes controlling photodynamics and energy transfer for advancing potential applications in molecular-based optoelectronic nanomaterials.

2. EXPERIMENTAL SECTION

2.1. GUMBOS and NanoGUMBOS Synthesis. Meso-tetra(4-carboxyphenyl)porphyrin (H_2-TCPP or TCPP) and zinc(II) meso-tetra(4-carboxyphenyl)porphyrin (Zn-TCPP) in acid form were purchased from Frontier Scientific. Trihexyl(tetradecyl)phosphonium chloride ([P66614][Cl]) and dichloromethane (DCM) were purchased from Sigma-Aldrich. Triply deionized ultrapure water was used for all samples. GUMBOS syntheses using a metathesis reaction were performed in a binary solvent mixture, as previously reported.[16] Briefly, TCPP or Zn-TCPP is neutralized using an excess of aqueous sodium hydroxide to obtain water-soluble tetrasodium salt in 10% excess. The other reactant [P66614][Cl] is dissolved in DCM. The two solutions are then mixed and stirred for 40 h. After the reaction is complete, the product is washed several times with water followed by removal of DCM using rotary evaporation under reduced pressure. Residual water is removed using freeze-drying and the final yield of the $[P66614]_4$[M-TCPP] GUMBOS product was approximately 96%. NanoGUMBOS are synthesized via reprecipitation of the GUMBOS in water by adding 50 μL of a 1 mM GUMBOS stock ethanolic solution into 5 mL of water under sonication for 30 min. The reaction scheme of the $[P66614]_4$[M-TCPP] GUMBOS is shown in Figure 1. Reprecipitation of $[P66614]_4$[M-TCPP] in water produces spherical nanoparticles with average sizes of 49 ± 25 nm for $[P66614]_4$[TCPP] nanoGUMBOS and 52 ± 15 nm for $[P66614]_4$[Zn-TCPP] nanoGUMBOS. Representative transmission electron microscopy (TEM) images of $[P66614]_4$[TCPP] and $[P66614]_4$[Zn-TCPP] nanoGUMBOS are shown in Figure 2a,b, respectively.

2.2. Transient Absorption. Ultrafast transient absorption spectroscopy is a powerful technique for investigation of excited-state relaxation dynamics of molecules and nanomaterials.[17,18] Our homebuilt transient absorption apparatus consists of an ultrafast laser system, an optical setup, and a fiber optic spectrometer detector. Laser pulses are generated

https://dx.doi.org/10.1021/acs.jpcc.0c08985
J. Phys. Chem. C 2020, 124, 24533−24541

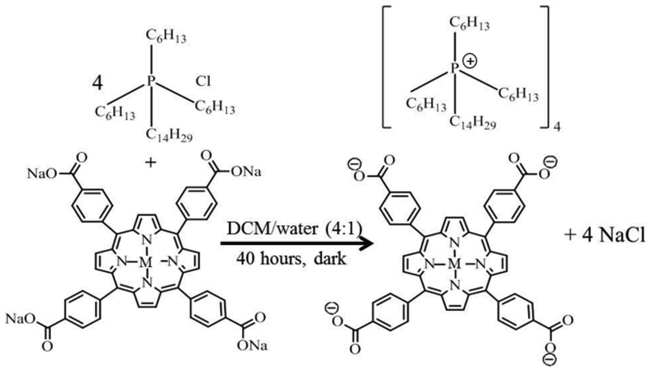

Figure 1. Reaction scheme of the synthesis of $[P66614]_4$[M-TCPP] GUMBOS.

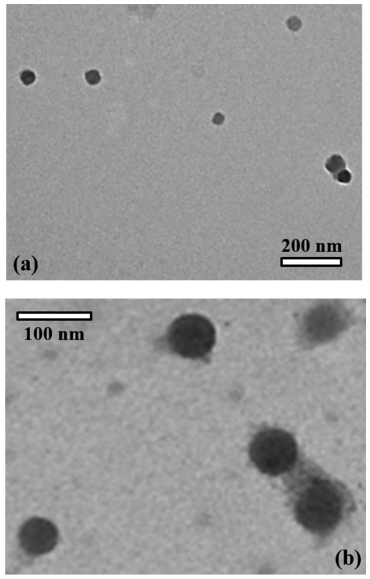

Figure 2. TEM images of (a) 50 nm $[P66614]_4$[TCPP] nanoGUMBOS and (b) 50 nm $[P66614]_4$[Zn-TCPP] nanoGUMBOS.

using a Titanium:sapphire laser system that produces 75 fs pulses centered at 800 nm with a 10 kHz repetition rate and an average power of 0.7 mJ/pulse. The initial laser beam is separated into pump and probe beams using a beam splitter. The 400 nm pump pulse beam is generated using frequency doubling by focusing the beam into a nonlinear beta barium borate crystal. An optical filter is then used to remove any 800 nm residual light yielding an excitation power of 0.16 μJ/pulse. Probe pulses are focused into a fused quartz flow cell containing water to generate femtosecond white light probe pulses. Pump and probe beams are refocused to a spatial overlap in the sample, which is contained in a 3 mm fused quartz flow cell. The pump-probe optical delay is controlled using a retroreflector on a computer-controlled translation stage for the pump beam. The temporal step sizes are all larger than the experimental temporal resolution, which is approximately 100 fs. Background spectra with probe only are subtracted from the pump-probe spectra using an automated beam block for each pump-probe time delay. Several spectral scans are acquired for each sample studied, and transient absorption spectra are acquired several times for statistical analysis.

3. RESULTS AND DISCUSSION

The extinction and fluorescence spectra of TCPP and Zn-TCPP molecular dyes and corresponding nanoGUMBOS are first measured for direct analysis and comparison. Figure 3a

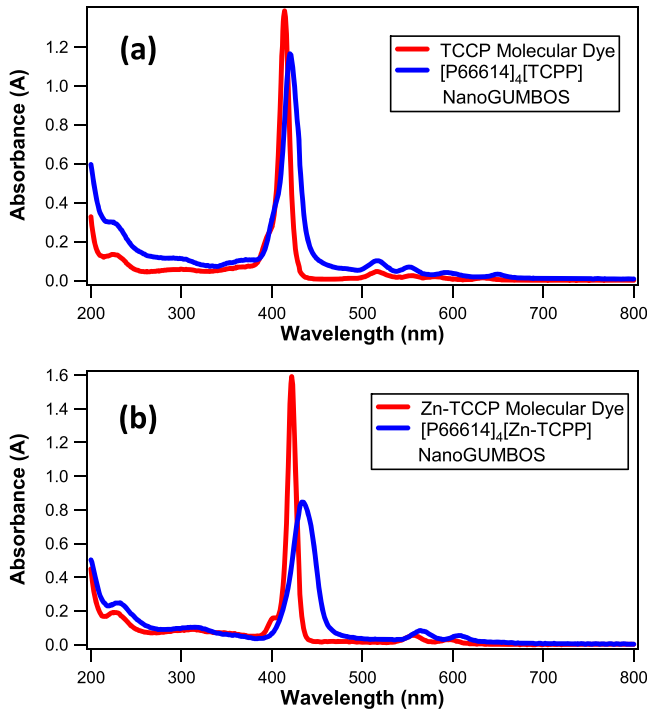

Figure 3. Absorbance spectra of (a) (red line) 10 μM TCPP molecular dye and (blue line) 10 μM $[P66614]_4$[TCPP] nanoGUMBOS and (b) (red line) 10 μM Zn-TCPP molecular dye and (blue line) 10 μM $[P66614]_4$[Zn-TCPP] nanoGUMBOS.

shows the absorbance spectra of the TCPP molecular dye and $[P66614]_4$[TCPP] nanoGUMBOS, with the Soret band corresponding to the S_0-S_2 transition[48] centered at 413 and 421 nm for the TCPP dye and $[P66614]_4$[TCPP] nanoGUMBOS, respectively. The absorbance spectra of the Zn-TCPP molecular dye and [Zn-TCPP]$[P66614]_4$ nanoGUMBOS are shown in Figure 3b, with the Soret band centered at 420 and 435 nm for the Zn-TCPP dye and $[P66614]_4$[Zn-TCPP] nanoGUMBOS, respectively. A redshift and broadening of the Soret band are observed in both $[P66614]_4$[TCPP] and $[P66614]_4$[Zn-TCPP] nanoGUMBOS, which are attributed to J-aggregation and a flattening of the porphyrin molecules in the nanoGUMBOS environment.[16,49,50] The Q bands, arising from the lower-energy S_0-S_1 transition, are centered after 500 nm for both dyes and both nanoGUMBOS samples. Due to the lower symmetry of porphyrin, the Q bands split into different components of unequal energies Q_x and Q_y with four different absorption peaks for TCPP centered around 516, 555, 581, and 633 nm.[51,52] For Zn-TCPP, the Q bands are degenerate in the D_{4h} symmetry and are centered around 556 and 596 nm. The Q bands have higher intensities and shift slightly in both nanoGUMBOS samples to around 516, 552, 594, and 650 nm in $[P66614]_4$[TCPP] nanoGUMBOS and around 565 and 607 nm in $[P66614]_4$[Zn-TCPP] nanoGUMBOS.

Fluorescence peaks observed in the molecular dyes and nanoGUMBOS are from $Q_x(0,0)$ and $Q_x(0,1)$ transitions.[43,44] The dominant relaxation channel of this Q_x transition is

https://dx.doi.org/10.1021/acs.jpcc.0c08985
J. Phys. Chem. C 2020, 124, 24533−24541

through intersystem crossing to the T_1 state, which has a very long lifetime on the order of microseconds to milliseconds.[53] Figure 4a is a display of the fluorescence spectra of the TCPP

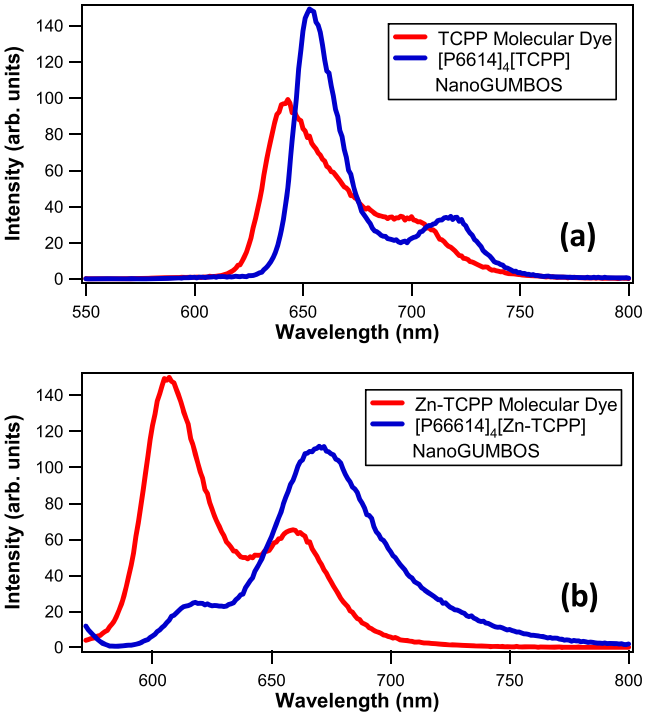

Figure 4. Fluorescence spectra of (a) (red line) 10 μM TCPP molecular dye in water and (blue line) 10 μM $[P66614]_4[TCPP]$ colloidal nanoGUMBOS after excitation at 420 nm and (b) (red line) 10 μM Zn-TCPP molecular dye in water and (blue line) 10 μM $[P66614]_4[Zn\text{-}TCPP]$ colloidal nanoGUMBOS after excitation at 420 nm.

molecular dye in water and $[P66614]_4[TCPP]$ nanoGUMBOS in water. The TCPP dye has a high intensity fluorescence band centered at 640 nm and a lower intensity band centered at 720 nm. In the case of $[P66614]_4[TCPP]$ nanoGUMBOS, the shorter-wavelength band is enhanced and red-shifted to 660 nm, while the longer-wavelength band is red-shifted to 725 nm. The fluorescence spectra of the Zn-TCPP molecular dye in water and $[P66614]_4[Zn\text{-}TCPP]$ nanoGUMBOS in water are shown in Figure 4b. The Zn-TCPP dye has a high-intensity fluorescence band centered at 610 nm and a lower-intensity band centered at 660 nm. In the case of $[P66614]_4[TCPP]$ nanoGUMBOS, the shorter-wavelength band is quenched and red-shifted to 625 nm, while the longer-wavelength band is enhanced and red-shifted to 680 nm. The absorbance and luminescence bands of TCPP and Zn-TCPP are red-shifted in nanoGUMBOS as compared to the corresponding free dye molecule in water due to the presence of the four bulky hydrophobic P66614 cations, leading to the formation of loosely packed aggregates in the nanoGUMBOS.[54]

Excited-state dynamics of different samples of M-TCPP molecular dyes are measured using transient absorption spectroscopy with 400 nm excitation pulses and results are compared to those of nanoGUMBOS samples. Figure 5a is a display of the transient absorption spectra of the 20 μM aqueous TCPP molecular dye in water. A negative band centered at 422 nm is due to depletion of the ground-state population, followed by a broad positive spectrum after 425

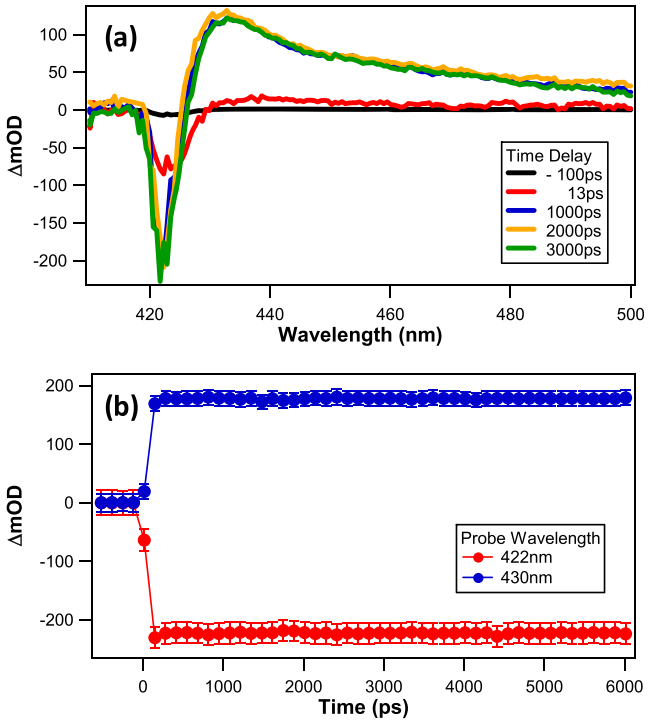

Figure 5. (a) Transient absorption spectra of 20 μM TCPP molecular dye in water at different time delays using 400 nm excitation. (b) Time profiles of the transient absorption spectra of aqueous TCPP molecular dye. The time-dependent signals are measured at 422 and 430 nm.

nm from excited-state absorption. An isosbestic point separating the ground-state depletion band and excited-state absorption region is observed at 424 nm. Representative time profiles of the transient absorption spectra of aqueous TCPP integrated at 422 and 430 nm are shown in Figure 5b. These time profiles change rapidly upon excitation due to S_2 to S_1 state internal conversion and then S_1 to triplet T_1 state intersystem crossing, both of which occur on faster timescales than the current experimental temporal resolution.[44] After these rapid transitions occur near time zero, the time profiles remain relatively constant due to a very long lifetime of the T_1 triplet state, which is significantly longer than the optical pump-probe time delays used in the experiment.[44]

Excited-state dynamics of $[P66614]_4[TCPP]$ nanoGUMBOS are studied and compared to those obtained from the TCPP molecular dye in order to understand aspects of the photophysical changes occurring due to the altered nanoGUMBOS environment. Figure 6a is a display of the transient absorption spectra of colloidal $[P66614]_4[TCPP]$ nanoGUMBOS at different time delays using 400 nm excitation pulses. A negative depletion band is centered at 423 nm followed by a broad positive spectrum from excited-state absorption after 440 nm. The two spectral features are separated by an isosbestic point at 438 nm. Representative time profiles of the transient absorption spectra of colloidal $[P66614]_4[TCPP]$ nanoGUMBOS integrated at 423 and 460 nm are shown in Figure 6b. As shown in Figure 6c, experimental data are fit with a global analysis technique using a sum of exponential functions.[17,18,55] The equation used in the global analysis fit is of the form $I(t) = y_0 + \sum_{i=1}^{n} A_i \exp\left(-\frac{t}{\tau_i}\right)$, where n is the number of

https://dx.doi.org/10.1021/acs.jpcc.0c08985
J. Phys. Chem. C 2020, 124, 24533−24541

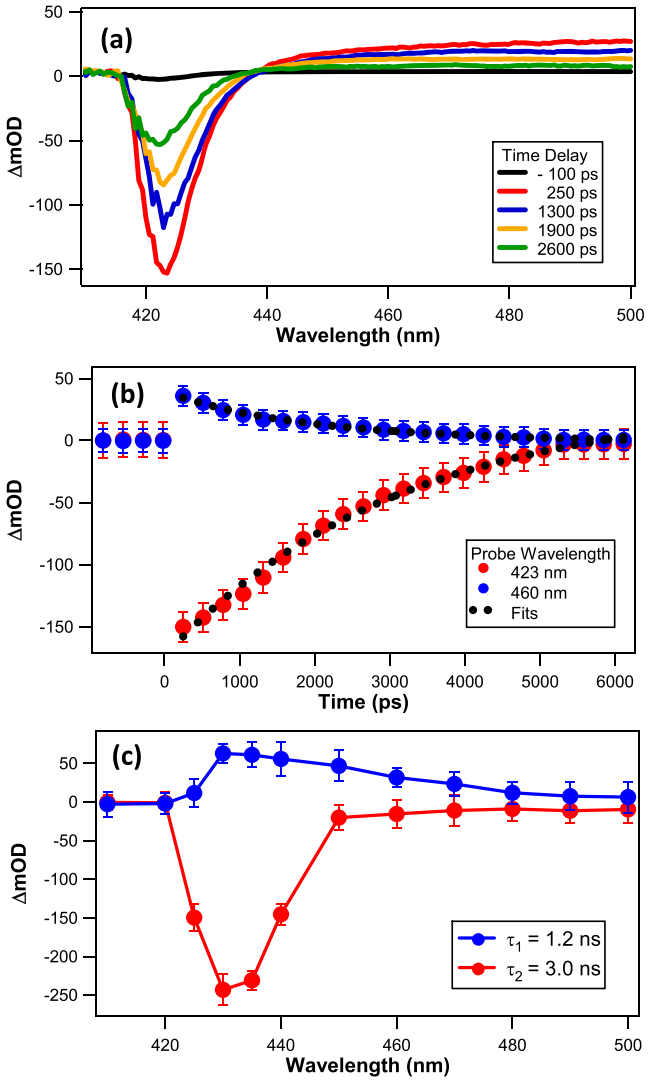

Figure 6. (a) Transient absorption spectra of colloidal $[P66614]_4[TCPP]$ nanoGUMBOS at different time delays using 400 nm excitation. (b) Time profiles of the transient absorption spectra of colloidal $[P66614]_4[TCPP]$ nanoGUMBOS. The time-dependent signals are measured at 423 nm and 460 nm. (c) Decay spectra obtained using a sum of exponential fits of time-dependent transient absorption spectra of colloidal $[P66614]_4[TCPP]$ nanoGUMBOS.

lifetimes required to accurately fit time profiles obtained from the transient absorption spectra. Two lifetimes are required to accurately fit the temporal evolution of the transient signal over the wavelength range of the experiment with lifetimes of τ_1 = 1.2 ± 0.1 ns and τ_2 = 3.0 ± 0.1 ns. The lifetimes are listed in Table 1. Transient absorption results demonstrate that excited-state dynamics of $[P66614]_4[TCPP]$ nanoGUMBOS are significantly faster than those of the aqueous TCPP dye. In

Table 1. Measured Lifetimes from $[P66614]_4[TCPP]$ NanoGUMBOS, Zn-TCPP, and $[P66614]_4[Zn\text{-}TCPP]$ NanoGUMBOS

$[P66614]_4[TCPP]$ nanoGUMBOS	Zn-TCPP	$[P66614]_4[Zn\text{-}TCPP]$ nanoGUMBOS
1.2 ± 0.1 ns	58 ± 4 ps	19 ± 1 ps
3.0 ± 0.1 ns	2.0 ± 0.2 ns	74 ± 6 ps

the nanoparticle, TCPP acts as an efficient energy donor and acceptor, with this pathway being greatly enhanced due to a closely packed nanoGUMBOS environment. A similar intermolecular energy transfer pathway was observed in our previous studies of $[Ru(bipy)_3][BETI]_2$ nanoGUMBOS.[17] Absorption and fluorescence investigations of porphyrin-clay complexes demonstrate related energy transfer pathways between nearby porphyrin molecules,[56,57] although the role of porphyrin aggregates in the nanoGUMBOS may further complicate this picture.[58] This type of intermolecular energy transfer can also be utilized in dye-sensitized solar cells,[21,26,28] using nanoGUMBOS attached to a semiconductor surface.

In $[P66614]_4[TCPP]$ nanoGUMBOS, the shorter lifetime of τ_1 is attributed to intermolecular energy transfer redistribution between nearby TCPP molecules, while the longer lifetime of τ_2 is ascribed to relaxation of the S_1 state (Q_x state) through intersystem crossing to the T_1 triplet state.[44] The decay spectrum corresponding to enhanced intersystem crossing in the $[P66614]_4[TCPP]$ nanoGUMBOS is dominated by ground-state depletion, as shown in Figure 6c, while the decay spectrum corresponding to energy transfer is dominated by excited-state absorption. Excited-state dynamics of the porphyrin are observed to be significantly faster in nanoGUMBOS than in the molecular dye alone, which is caused by a combination of energy transfer and enhanced intersystem crossing in the nanomaterial environment, leading to dramatically altered photophysical properties of the nanoGUMBOS.[59,60]

The effect of the zinc metal center on the excited-state dynamics of aqueous Zn-TCPP and colloidal $[P66614]_4[Zn\text{-}TCPP]$ nanoGUMBOS is also investigated. Here, the presence of a Zn metal center significantly decreases the excited-state lifetimes in the Zn-TCPP molecular dye as compared to the TCPP molecular dye due to increased spin−orbit coupling and electronic delocalization in Zn-TCPP.[43,44,61] Additionally, a heavy metal center in organometallic molecules is known to accelerate intersystem crossing from triplet to singlet states.[62−64] Figure 7a is a display of the transient absorption spectra of the aqueous Zn-TCPP molecular dye at different time delays using 400 nm excitation pulses. A negative ground-state depletion band is centered at 426 nm, followed by a positive broad spectrum after 435 nm due to excited-state absorption. The two spectral regions are separated by an isosbestic point at 433 nm. Representative time traces from the transient absorption spectra integrated at 428 and 450 nm are shown in Figure 7b. Analyses of these time traces demonstrate that these relaxation dynamics are described using a single lifetime of τ_3 = 2.0 ± 0.2 ns. This lifetime is attributed to relaxation of the S_1 state (Q_x state) to the triplet T_1 state through intersystem crossing. Previous studies on the upconversion fluorescence spectroscopy of a similar dye molecule, zinc tetraphenylporphyrin (ZnTPP), in benzene describe a similar lifetime of 1.7 ns.[43] In our measurements, the slightly different zinc-porphyrin molecular structure in a different highly polar aqueous solvent causes a longer relaxation lifetime for this intersystem crossing transition.

Transient absorption of the Zn-TCPP molecular dye is also studied under higher temporal resolution, using smaller pump-probe time delay steps, with all other experimental conditions being the same. Representative transient absorption spectra under higher temporal resolution are shown in Figure 7c, where the relative intensity of the ground-state depletion is greater than the corresponding spectra shown in Figure 7b at

https://dx.doi.org/10.1021/acs.jpcc.0c08985
J. Phys. Chem. C 2020, 124, 24533−24541

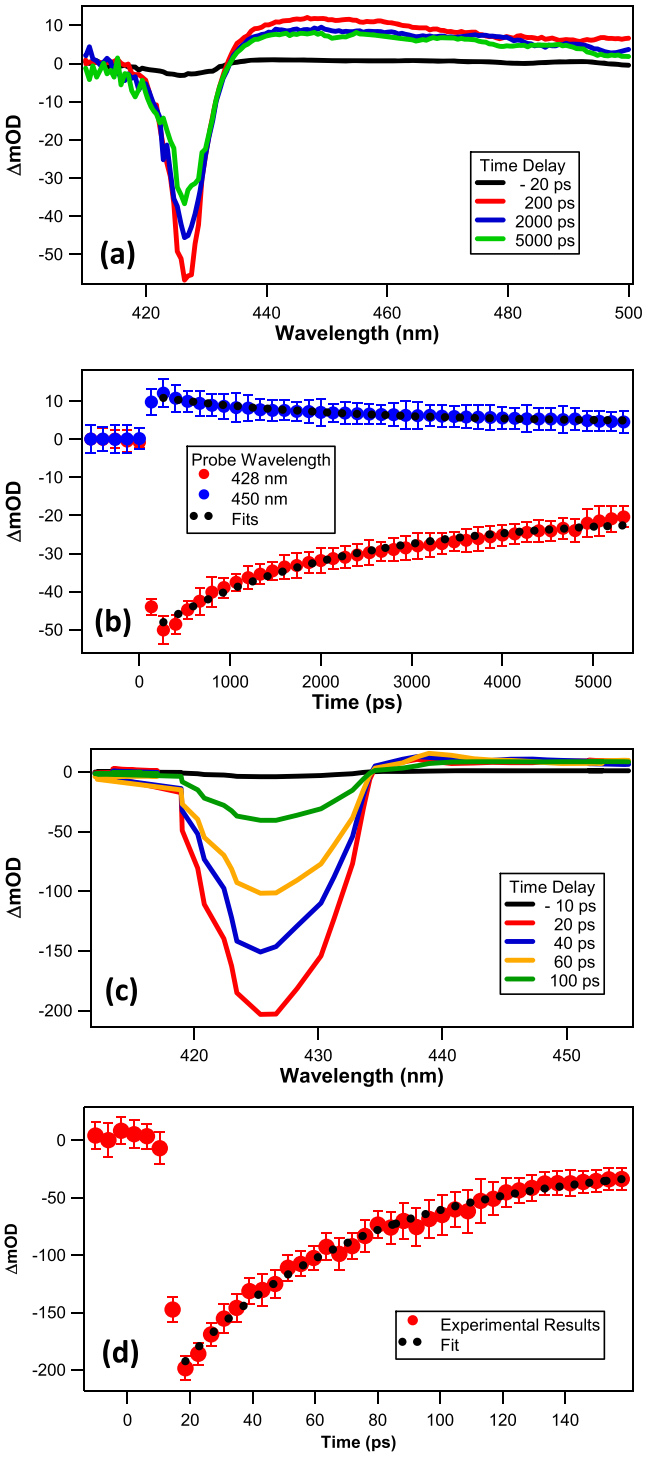

Figure 7. (a) Transient absorption spectra of 20 μL of aqueous Zn-TCPP molecular dye at different time delays using 400 nm excitation. (b) Time profiles of the transient absorption spectra of aqueous Zn-TCPP molecular dye. The time-dependent signals are measured at 428 and 450 nm. (c) Transient absorption spectra of 20 μL of aqueous Zn-TCPP molecular dye at different time delays at short time steps using 400 nm excitation. (d) Time profiles of Zn-TCPP molecular dye at short time delays integrated at 425 nm.

longer delay times. The time profile of the Zn-TCPP molecular dye in water at short time delays integrated at 425 nm is shown in Figure 7d and can be fit with a single exponential lifetime of $\tau_4 = 58 \pm 4$ ps, which is attributed to the vibrational relaxation of the S_1 excited-state population, after internal conversion from the S_2 state.[43,44] The lifetimes measured from Zn-TCPP are also listed in Table 1. Previous transient absorption studies on a similar dye molecule, ZnTPP, in benzene and DCM measured lifetimes of vibrational relaxation of the S_1 state to be approximately 12 and 38 ps, respectively. In that case, solvent interaction was found to play an important role in these dynamics.[43] Here, the slightly different molecular structure of Zn-TCPP in a different solvent (water) shows a significantly longer lifetime where an overall trend of increasing lifetimes for solvents of increasing polarity is observed. Internal conversion from the excited S_2 to S_1 states, which is expected to occur on timescales of approximately 1 ps,[43] is faster than the current experimental temporal resolution conditions employed.

Transient absorption spectroscopy measurements are also performed on colloidal $[P66614]_4[Zn\text{-}TCPP]$ nanoGUMBOS. Figure 8a is a display of the transient absorption spectra of

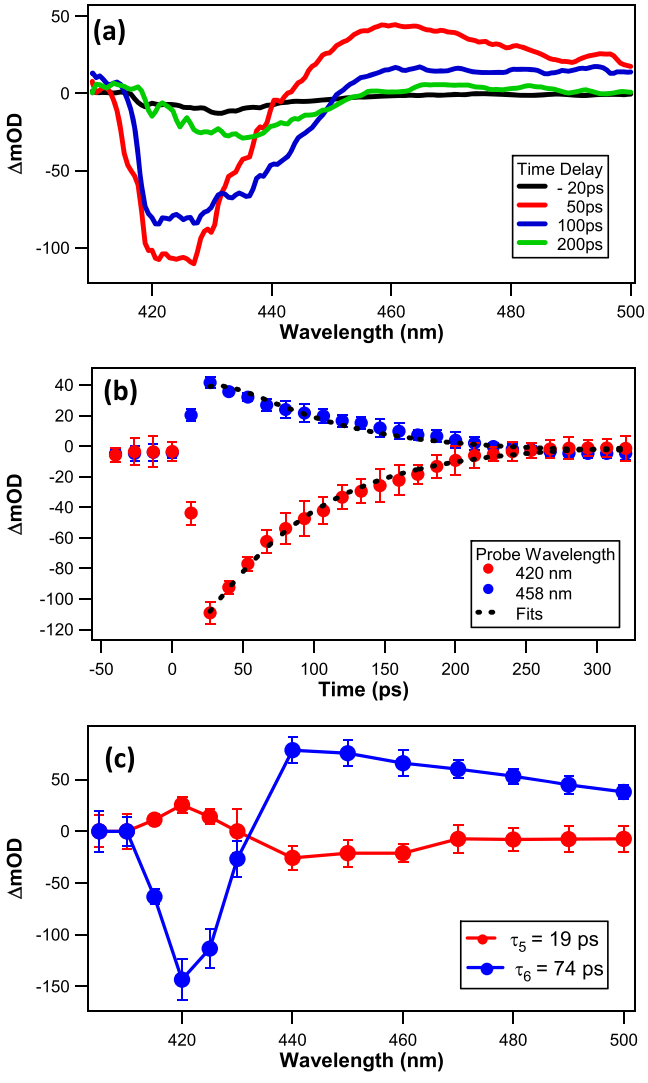

Figure 8. (a) Transient absorption spectra of colloidal $[P66614]_4[Zn\text{-}TCPP]$ nanoGUMBOS at different time delays using 400 nm excitation. (b) Time profiles of the transient absorption spectra of colloidal $[P66614]_4[Zn\text{-}TCPP]$ nanoGUMBOS. The time-dependent signals are measured at 428 and 450 nm. (c) Decay spectra obtained using a sum of exponential fits of time-dependent transient absorption spectra of colloidal $[P66614]_4[Zn\text{-}TCPP]$ nanoGUMBOS.

https://dx.doi.org/10.1021/acs.jpcc.0c08985
J. Phys. Chem. C 2020, 124, 24533−24541

colloidal $[P66614]_4[Zn\text{-}TCPP]$ nanoGUMBOS at different time delays using 400 nm excitation. A ground-state depletion band is centered at 425 nm, followed by a broad excited-state absorption spectrum after 450 nm. Time-dependent transient absorption spectra integrated at 420 and 458 nm are shown in Figure 8b. Corresponding decay spectra from global analyses of the time profiles are shown in Figure 8c. Time profiles are fit using a sum of two exponential functions with lifetimes $\tau_5 = 19 \pm 1$ ps and $\tau_6 = 74 \pm 6$ ps. These lifetimes are also listed in Table 1 for comparison. The faster lifetime τ_5 is attributed to energy transfer between nearby Zn-TCPP molecules in the nanoGUMBOS environment because this lifetime and corresponding decay spectrum are not observed in the Zn-TCPP molecular dye alone in water. The slower lifetime τ_6 is ascribed primarily to intersystem crossing of the S_1 state to the T_1 state, since the corresponding decay spectrum is dominated by ground-state depletion near 420 nm, with the transient absorption spectra approximately equal to zero within experimental uncertainty after the decay of this τ_6 signal. Here, the presence of the intermolecular energy transfer pathway also increases the rate of relaxation of the S_1 state in the nanoGUMBOS material caused by a larger degree of electronic delocalization in the nanoGUMBOS environment. In contrast to the decay spectrum of energy transfer in the $[P66614]_4[TCPP]$ nanoGUMBOS, which is dominated by excited-state absorption, the decay spectrum of energy transfer in $[P66614]_4[Zn\text{-}TCPP]$ nanoGUMBOS has both the positive excited-state absorption character near 420 nm and negative ground-state depletion character near 450 nm.

By comparing these results to our previous work on $[Ru(bipy)_3][BETI]_2$ nanoGUMBOS[17] and [BG][BETI] nanoGUMBOS,[18] several important conclusions can be obtained. The $[Ru(bipy)_3][BETI]_2$ nanoGUMBOS have a crystalline structure, resulting in phonon oscillations. The porphyrin-based nanoGUMBOS described here are amorphous in structure, so no phonon oscillations are observed. Additionally, the role of the Zn metal center is directly observed to significantly decrease the energy transfer lifetime in $[P66614]_4[Zn\text{-}TCPP]$ nanoGUMBOS as compared to $[P66614]_4[TCPP]$ nanoGUMBOS, where the Zn metal center is not present. Such comparisons were not possible in the $[Ru(bipy)_3][BETI]_2$ nanoGUMBOS study due to the different chemical structure of the parent dye molecule. For both the porphyrin nanoGUMBOS and the $[Ru(bipy)_3][BETI]_2$ nanoGUMBOS, where intersystem crossing to triplet states occurs, the excited-state dynamics have faster lifetimes than the corresponding parent dye molecules due primarily to the added energy transfer pathways. However, for the [BG][BETI] nanoGUMBOS, which have much faster dynamics with no intersystem crossing, the excited-state dynamics are slower than in the corresponding parent dye molecules due to molecular hindrance. These transient absorption results of porphyrin and zinc-porphyrin molecular dyes and comparisons to corresponding nanoGUMBOS provide key information on altered photodynamic properties in molecular-based nanomaterials for enhancing energy transfer and excited-state relaxation in potential optoelectronic applications.

4. CONCLUSIONS

Ultrafast relaxation dynamics of colloidal porphyrin- and zinc porphyrin-based nanomaterials are studied using transient absorption spectroscopy, showing dramatically faster lifetimes and altered spectra as compared to corresponding parent dye molecules in water. $[P66614]_4[TCPP]$ and $[P66614]_4[Zn\text{-}TCPP]$ nanoGUMBOS are prepared using a metathesis reaction, resulting in 50 nm nanospheres in stable aqueous colloidal suspension. Transient absorption spectroscopy studies of TCPP and Zn-TCPP molecular dyes in water using 400 nm excitation display long-lived excited states from intersystem crossing of the S_1 state to the triplet T_1 state. Corresponding nanoGUMBOS show dramatically faster relaxation dynamics with an additional pathway due to intermolecular energy transfer in the altered nanoGUMBOS environment, which is characterized by close-packing aggregates of the porphyrin and P66614 molecular ions. In addition, Zn-porphyrin nanoGUMBOS demonstrate very efficient relaxation dynamics and energy transfer caused by increased electronic delocalization and spin−orbit coupling from the Zn metal center. This highly efficient energy transfer pathway is very promising for potential applications in photovoltaics and optoelectronics. These studies also provide fundamental insights into ultrafast photodynamics for advancing optoelectronic technologies utilizing molecular-based nanomaterials.

AUTHOR INFORMATION

Corresponding Author

Louis H. Haber − *Department of Chemistry, Louisiana State University, Baton Rouge, Louisiana 70803, United States;* orcid.org/0000-0001-7706-7789; Email: lhaber@lsu.edu

Authors

Tony E. Karam − *Department of Chemistry, Louisiana State University, Baton Rouge, Louisiana 70803, United States*

Noureen Siraj − *Department of Chemistry, Louisiana State University, Baton Rouge, Louisiana 70803, United States*

Jeewan C. Ranasinghe − *Department of Chemistry, Louisiana State University, Baton Rouge, Louisiana 70803, United States*

Paulina E. Kolic − *Department of Chemistry, Louisiana State University, Baton Rouge, Louisiana 70803, United States*

Bishnu P. Regmi − *Department of Chemistry, Louisiana State University, Baton Rouge, Louisiana 70803, United States;* orcid.org/0000-0001-7690-9825

Isiah M. Warner − *Department of Chemistry, Louisiana State University, Baton Rouge, Louisiana 70803, United States;* orcid.org/0000-0002-5336-7653

Complete contact information is available at: https://pubs.acs.org/10.1021/acs.jpcc.0c08985

Notes

The authors declare no competing financial interest.

ACKNOWLEDGMENTS

Generous financial support for this work was provided by Louisiana State University. L.H.H. and J.C.R. gratefully acknowledge financial support from the National Science Foundation EPSCoR CIMM project under award OIA-1541079. N.S. gratefully acknowledges financial support from the National Science Foundation under award OIA-1833004. I.M.W. gratefully acknowledges financial support through NASA cooperative agreement NNX 16AQ93A under contract number NASA/LEQSF (2016-19)-Phase 3-10 and the National Science Foundation under grant no. CHE-1905105. Any opinions, findings, and conclusions, or recommendations expressed in this material are those of the author(s) and do not necessarily reflect the views of the National Science Foundation. Preliminary analyses of these results are also

included in TEK's thesis at LSU, "Ultrafast and Nonlinear Spectroscopy of Colloidal Nanomaterials" in 2016. Use of LSU Shared Instrumentation Facility is also acknowledged.

REFERENCES

(1) Yang, K.; Xu, H.; Cheng, L.; Sun, C.; Wang, J.; Liu, Z. In vitro and in vivo near-infrared photothermal therapy of cancer using polypyrrole organic nanoparticles. *Adv. Mater.* **2012**, *24*, 5586−5592.
(2) Yang, J.; Choi, J.; Bang, D.; Kim, E.; Lim, E.-K.; Park, H.; Suh, J.-S.; Lee, K.; Yoo, K.-H.; Kim, E.-K.; Huh, Y.-M.; Haam, S. Convertible organic nanoparticles for near-infrared photothermal ablation of cancer cells. *Angew. Chem., Int. Ed.* **2011**, *50*, 441−444.
(3) Petkau, K.; Kaeser, A.; Fischer, I.; Brunsveld, L.; Schenning, A. P. H. J. Pre- and postfunctionalized self-assembled π-conjugated fluorescent organic nanoparticles for dual targeting. *J. Am. Chem. Soc.* **2011**, *133*, 17063−17071.
(4) An, B.-K.; Kwon, S.-K.; Jung, S.-D.; Park, S. Y. Enhanced emission and its switching in fluorescent organic nanoparticles. *J. Am. Chem. Soc.* **2002**, *124*, 14410−14415.
(5) Warner, I. M.; El-Zahab, B.; Siraj, N. Perspectives on Moving Ionic Liquid Chemistry into the Solid Phase. *Anal. Chem.* **2014**, *86*, 7184−7191.
(6) Bwambok, D. K.; El-Zahab, B.; Challa, S. K.; Li, M.; Chandler, L.; Baker, G. A.; Warner, I. M. Near-Infrared Fluorescent Nano-GUMBOS for Biomedical Imaging. *ACS Nano* **2009**, *3*, 3854−3860.
(7) Cole, M. R.; Li, M.; Jadeja, R.; El-Zahab, B.; Hayes, D.; Hobden, J. A.; Janes, M. E.; Warner, I. M. Minimizing human infection from Escherichia coli O157: H7 using GUMBOS. *J. Antimicrob. Chemother.* **2013**, *68*, 1312−1318.
(8) Cole, M. R.; Li, M.; El-Zahab, B.; Janes, M. E.; Hayes, D.; Warner, I. M. Design, Synthesis, and Biological Evaluation of β-Lactam Antibiotic-Based Imidazolium-and Pyridinium-Type Ionic Liquids. *Chem. Biol. Drug Des.* **2011**, *78*, 33−41.
(9) Magut, P. K. S.; Das, S.; Fernand, V. E.; Losso, J.; McDonough, K.; Naylor, B. M.; Aggarwal, S.; Warner, I. M. Tunable cytotoxicity of rhodamine 6G via anion variations. *J. Am. Chem. Soc.* **2013**, *135*, 15873−15879.
(10) Das, S.; Magut, P. K. S.; de Rooy, S. L.; Hasan, F.; Warner, I. M. Ionic liquid-based fluorescein colorimetric pH nanosensors. *RSC Adv.* **2013**, *3*, 21054−21061.
(11) Lu, C.; Das, S.; Magut, P. K. S.; Li, M.; El-Zahab, B.; Warner, I. M. Irradiation induced fluorescence enhancement in PEGylated cyanine-based NIR nano- and mesoscale GUMBOS. *Langmuir* **2012**, *28*, 14415−14423.
(12) Regmi, B. P.; Monk, J.; El-Zahab, B.; Das, S.; Hung, F. R.; Hayes, D. J.; Warner, I. M. A novel composite film for detection and molecular weight determination of organic vapors. *J. Mater. Chem.* **2012**, *22*, 13732−13741.
(13) Das, S.; Bwambok, D.; El-Zahab, B.; Monk, J.; de Rooy, S. L.; Challa, S.; Li, M.; Hung, F. R.; Baker, G. A.; Warner, I. M. Nontemplated approach to tuning the spectral properties of cyanine-based fluorescent nanoGUMBOS. *Langmuir* **2010**, *26*, 12867−12876.
(14) Siraj, N.; Hasan, F.; Das, S.; Kiruri, L. W.; Steege Gall, K. E.; Baker, G. A.; Warner, I. M. Carbazole-derived group of uniform materials based on organic salts: solid state fluorescent analogues of ionic liquids for potential applications in organic-based blue light-emitting diodes. *J. Phys. Chem. C* **2014**, *118*, 2312−2320.
(15) Jordan, A. N.; Das, S.; Siraj, N.; de Rooy, S. L.; Li, M.; El-Zahab, B.; Chandler, L.; Baker, G. A.; Warner, I. M. Anion-controlled morphologies and spectral features of cyanine-based nanoGUMBOS − an improved photosensitizer. *Nanoscale* **2012**, *4*, 5031−5038.
(16) Kolic, P. E.; Siraj, N.; Hamdan, S.; Regmi, B. P.; Warner, I. M. Synthesis and Characterization of Porphyrin-Based GUMBOS and NanoGUMBOS as Improved Photosensitizers. *J. Phys. Chem. C* **2016**, *120*, 5155−5163.
(17) Karam, T. E.; Siraj, N.; Warner, I. M.; Haber, L. H. Anomalous size-dependent excited-state relaxation dynamics of NanoGUMBOS. *J. Phys. Chem. C* **2015**, *119*, 28206−28213.
(18) Karam, T. E.; Siraj, N.; Zhang, Z.; Ezzir, A. F.; Warner, I. M.; Haber, L. H. Ultrafast and nonlinear spectroscopy of brilliant green-based nanoGUMBOS with enhanced near-infrared emission. *J. Chem. Phys.* **2017**, *147*, 144701.
(19) Yella, A.; Lee, H.-W.; Tsao, H. N.; Yi, C.; Chandiran, A. K.; Nazeeruddin, M. K.; Diau, E. W.-G.; Yeh, C.-Y.; Zakeeruddin, S. M.; Grätzel, M. Porphyrin-sensitized solar cells with cobalt (II/III)−based redox electrolyte exceed 12 percent efficiency. *Science* **2011**, *334*, 629−634.
(20) Bessho, T.; Zakeeruddin, S. M.; Yeh, C.-Y.; Diau, E. W.-G.; Grätzel, M. Highly efficient mesoscopic dye-sensitized solar cells based on donor−acceptor-substituted porphyrins. *Angew. Chem., Int. Ed.* **2010**, *49*, 6646−6649.
(21) Negre, C. F. A.; Milot, R. L.; Martini, L. A.; Ding, W.; Crabtree, R. H.; Schmuttenmaer, C. A.; Batista, V. S. Efficiency of interfacial electron transfer from Zn-porphyrin dyes into TiO_2 correlated to the linker single molecule conductance. *J. Phys. Chem. C* **2013**, *117*, 24462−24470.
(22) Li, L.-L.; Diau, E. W.-G. Porphyrin-sensitized solar cells. *Chem. Soc. Rev.* **2013**, *42*, 291−304.
(23) Wasielewski, M. R. Self-assembly strategies for integrating light harvesting and charge separation in artificial photosynthetic systems. *Acc. Chem. Res.* **2009**, *42*, 1910−1921.
(24) Choi, M.-S.; Yamazaki, T.; Yamazaki, I.; Aida, T. Bioinspired molecular design of light-harvesting multiporphyrin arrays. *Angew. Chem., Int. Ed.* **2004**, *43*, 150−158.
(25) Mickley Conron, S. M.; Shoer, L. E.; Smeigh, A. L.; Ricks, A. B.; Wasielewski, M. R. Photoinitiated electron transfer in zinc porphyrin−perylenediimide cruciforms and their self-assembled oligomers. *J. Phys. Chem. B* **2013**, *117*, 2195−2204.
(26) Mozer, A. J.; Griffith, M. J.; Tsekouras, G.; Wagner, P.; Wallace, G. G.; Mori, S.; Sunahara, K.; Miyashita, M.; Earles, J. C.; Gordon, K. C.; Du, L.; Katoh, R.; Furube, A.; Officer, D. L. Zn− Zn porphyrin dimer-sensitized solar cells: toward 3-D light harvesting. *J. Am. Chem. Soc.* **2009**, *131*, 15621−15623.
(27) Du, B.; Fortin, D.; Harvey, P. D. Singlet and Triplet Energy Transfers in Tetra-(meso-truxene) zinc (II)-and Tetra-(meso-tritruxene) zinc (II) Porphyrin and Porphyrin-Free Base Dendrimers. *Inorg. Chem.* **2011**, *50*, 11493−11505.
(28) Lu, H.-P.; Tsai, C.-Y.; Yen, W.-N.; Hsieh, C.-P.; Lee, C.-W.; Yeh, C.-Y.; Diau, E. W.-G. Control of dye aggregation and electron injection for highly efficient porphyrin sensitizers adsorbed on semiconductor films with varying ratios of coadsorbate. *J. Phys. Chem. C* **2009**, *113*, 20990−20997.
(29) Uetomo, A.; Kozaki, M.; Suzuki, S.; Yamanaka, K.-i.; Ito, O.; Okada, K. Efficient light-harvesting antenna with a multi-porphyrin cascade. *J. Am. Chem. Soc.* **2011**, *133*, 13276−13279.
(30) Hasobe, T. Porphyrin-based supramolecular nanoarchitectures for solar energy conversion. *J. Phys. Chem. Lett.* **2013**, *4*, 1771−1780.
(31) Hippius, C.; van Stokkum, I. H. M.; Gsänger, M.; Groeneveld, M. M.; Williams, R. M.; Würthner, F. Sequential FRET processes in calix[4]arene-linked orange-red-green perylene bisimide dye zigzag arrays. *J. Phys. Chem. C* **2008**, *112*, 2476−2486.
(32) Diring, S.; Puntoriero, F.; Nastasi, F.; Campagna, S.; Ziessel, R. Star-shaped multichromophoric arrays from bodipy dyes grafted on truxene core. *J. Am. Chem. Soc.* **2009**, *131*, 6108−6110.
(33) Fenwick, O.; Sprafke, J. K.; Binas, J.; Kondratuk, D. V.; Di Stasio, F.; Anderson, H. L.; Cacialli, F. Linear and cyclic porphyrin hexamers as near-infrared emitters in organic light-emitting diodes. *Nano Lett.* **2011**, *11*, 2451−2456.
(34) Pandey, R. K.; Bellnier, D. A.; Smith, K. M.; Dougherty, T. J. Chlorin and porphyrin derivatives as potential photosensitizers in photodynamic therapy. *Photochem. Photobiol.* **1991**, *53*, 65−72.
(35) Ethirajan, M.; Chen, Y.; Joshi, P.; Pandey, R. K. The role of porphyrin chemistry in tumor imaging and photodynamic therapy. *Chem. Soc. Rev.* **2011**, *40*, 340−362.
(36) O'Connor, A. E.; Gallagher, W. M.; Byrne, A. T. Porphyrin and nonporphyrin photosensitizers in oncology: preclinical and clinical

https://dx.doi.org/10.1021/acs.jpcc.0c08985
J. Phys. Chem. C 2020, 124, 24533−24541

advances in photodynamic therapy. *Photochem. Photobiol.* **2009**, *85*, 1053−1074.
(37) Kessel, D.; Luguya, R.; Vicente, M. G. H. Localization and Photodynamic Efficacy of Two Cationic Porphyrins Varying in Charge Distribution. *Photochem. Photobiol.* **2003**, *78*, 431−435.
(38) Lin, S.; Diercks, C. S.; Zhang, Y.-B.; Kornienko, N.; Nichols, E. M.; Zhao, Y.; Paris, A. R.; Kim, D.; Yang, P.; Yaghi, O. M.; Chang, C. J. Covalent organic frameworks comprising cobalt porphyrins for catalytic CO_2 reduction in water. *Science* **2015**, *349*, 1208−1213.
(39) Hod, I.; Sampson, M. D.; Deria, P.; Kubiak, C. P.; Farha, O. K.; Hupp, J. T. Fe-porphyrin-based metal−organic framework films as high-surface concentration, heterogeneous catalysts for electrochemical reduction of CO_2. *ACS Catal.* **2015**, *5*, 6302−6309.
(40) Maeda, C.; Taniguchi, T.; Ogawa, K.; Ema, T. Bifunctional Catalysts Based on m-Phenylene-Bridged Porphyrin Dimer and Trimer Platforms: Synthesis of Cyclic Carbonates from Carbon Dioxide and Epoxides. *Angew. Chem., Int. Ed.* **2015**, *54*, 134−138.
(41) Omagari, T.; Suzuki, A.; Akita, M.; Yoshizawa, M. Efficient catalytic epoxidation in water by axial N-ligand-free Mn-porphyrins within a micellar capsule. *J. Am. Chem. Soc.* **2016**, *138*, 499−502.
(42) Charvet, R.; Yamamoto, Y.; Sasaki, T.; Kim, J.; Kato, K.; Takata, M.; Saeki, A.; Seki, S.; Aida, T. Segregated and alternately stacked donor/acceptor nanodomains in tubular morphology tailored with zinc porphyrin−C_{60} amphiphilic dyads: clear geometrical effects on photoconduction. *J. Am. Chem. Soc.* **2012**, *134*, 2524−2527.
(43) Yu, H.-Z.; Baskin, J. S.; Zewail, A. H. Ultrafast dynamics of porphyrins in the condensed phase: II. Zinc tetraphenylporphyrin. *J. Phys. Chem. A* **2002**, *106*, 9845−9854.
(44) Baskin, J. S.; Yu, H.-Z.; Zewail, A. H. Ultrafast dynamics of porphyrins in the condensed phase: I. Free base tetraphenylporphyrin. *J. Phys. Chem. A* **2002**, *106*, 9837−9844.
(45) Steiger, B.; Baskin, J. S.; Anson, F. C.; Zewail, A. H. Femtosecond Dynamics of Dioxygen − Picket-Fence Cobalt Porphyrins: Ultrafast Release of O_2 and the Nature of Dative Bonding. *Angew. Chem., Int. Ed.* **2000**, *39*, 257−260.
(46) Yu, H.-Z.; Baskin, J. S.; Steiger, B.; Anson, F. C.; Zewail, A. H. Femtosecond dynamics and electrocatalysis of the reduction of O_2: tetraruthenated cobalt porphyrins. *J. Am. Chem. Soc.* **1999**, *121*, 484−485.
(47) Yu, H. Z.; Baskin, J. S.; Steiger, B.; Wan, C. Z.; Anson, F. C.; Zewail, A. H. Femtosecond dynamics of metalloporphyrins: electron transfer and energy redistribution. *Chem. Phys. Lett.* **1998**, *293*, 1−8.
(48) Shirakawa, M.; Fujita, N.; Shinkai, S. A stable single piece of unimolecularly π-stacked porphyrin aggregate in a thixotropic low molecular weight gel: a one-dimensional molecular template for polydiacetylene wiring up to several tens of micrometers in length. *J. Am. Chem. Soc.* **2005**, *127*, 4164−4165.
(49) Ishida, Y.; Masui, D.; Shimada, T.; Tachibana, H.; Inoue, H.; Takagi, S. The mechanism of the porphyrin spectral shift on inorganic nanosheets: the molecular flattening induced by the strong host−guest interaction due to the "size-matching rule". *J. Phys. Chem. C* **2012**, *116*, 7879−7885.
(50) Hestand, N. J.; Spano, F. C. Expanded theory of H- and J-molecular aggregates: the effects of vibronic coupling and intermolecular charge transfer. *Chem. Rev.* **2018**, *118*, 7069−7163.
(51) Dorough, G. D.; Miller, J. R.; Huennekens, F. M. Spectra of the Metallo-derivatives of $\alpha,\beta,\gamma,\delta$-Tetraphenylporphine. *J. Am. Chem. Soc.* **1951**, *73*, 4315−4320.
(52) Thomas, D. W.; Martell, A. E. Absorption Spectra of para-Substituted Tetraphenylporphines1, 2. *J. Am. Chem. Soc.* **1956**, *78*, 1338−1343.
(53) Pekkarinen, L.; Linschitz, H. Studies on Metastable States of Porphyrins. II. Spectra and Decay Kinetics of Tetraphenylporphine, Zinc Tetraphenylporphine and Bacteriochlorophyll[1]. *J. Am. Chem. Soc.* **1960**, *82*, 2407−2411.
(54) Zimmerman, J. D.; Diev, V. V.; Hanson, K.; Lunt, R. R.; Yu, E. K.; Thompson, M. E.; Forrest, S. R. Porphyrin-Tape/C_{60} Organic Photodetectors with 6.5% External Quantum Efficiency in the Near Infrared. *Adv. Mater.* **2010**, *22*, 2780−2783.
(55) Karam, T. E.; Khoury, R. A.; Haber, L. H. Excited-state dynamics of size-dependent colloidal TiO_2-Au nanocomposites. *J. Chem. Phys.* **2016**, *144*, 124704.
(56) Takagi, S.; Tryk, D. A.; Inoue, H. Photochemical energy transfer of cationic porphyrin complexes on clay surface. *J. Phys. Chem. B* **2002**, *106*, 5455−5460.
(57) Takagi, S.; Eguchi, M.; Tryk, D. A.; Inoue, H. Light-harvesting energy transfer and subsequent electron transfer of cationic porphyrin complexes on clay surfaces. *Langmuir* **2006**, *22*, 1406−1408.
(58) Brixner, T.; Hildner, R.; Köhler, J.; Lambert, C.; Würthner, F. Exciton transport in molecular aggregates−from natural antennas to synthetic chromophore systems. *Adv. Energy Mater.* **2017**, *7*, 1700236.
(59) Fita, P.; Fedoseeva, M.; Vauthey, E. Ultrafast Excited-State Dynamics of Eosin B: a Potential Probe of the Hydrogen-Bonding Properties of the Environment. *J. Phys. Chem. A* **2011**, *115*, 2465−2470.
(60) Zhao, Q.; Wang, Y.; Xu, Y.; Yan, Y.; Huang, J. Out-of-plane coordinated porphyrin nanotubes with enhanced singlet oxygen generation efficiency. *Sci. Rep.* **2016**, *6*, 31339.
(61) Penfold, T. J.; Gindensperger, E.; Daniel, C.; Marian, C. M. Spin-vibronic mechanism for intersystem crossing. *Chem. Rev.* **2018**, *118*, 6975−7025.
(62) Turro, N. J.; Ramamurthy, V.; Ramamurthy, V.; Scaiano, J. C. *Principles of molecular photochemistry: an introduction*; University science books: 2009.
(63) Zhao, Q.; Huang, C.; Li, F. Phosphorescent heavy-metal complexes for bioimaging. *Chem. Soc. Rev.* **2011**, *40*, 2508−2524.
(64) Chergui, M. Ultrafast photophysics of transition metal complexes. *Acc. Chem. Res.* **2015**, *48*, 801−808.

https://dx.doi.org/10.1021/acs.jpcc.0c08985
J. Phys. Chem. C 2020, 124, 24533−24541